

# Temporal Pair Consistency for Variance-Reduced Flow Matching

Chika Maduabuchi<sup>1</sup> Jindong Wang<sup>1</sup>

## Abstract

Continuous-time generative models—such as diffusion models, flow matching, and rectified flow—learn time-dependent vector fields but are typically trained with objectives that treat timesteps independently, leading to high estimator variance and inefficient sampling. Prior approaches mitigate this via explicit smoothness penalties, trajectory regularization, or modified probability paths and solvers. We introduce *Temporal Pair Consistency* (TPC), a lightweight variance-reduction principle that instead couples velocity predictions at paired timesteps along the same probability path, operating entirely at the estimator level without modifying the model architecture, probability path, or solver. We provide a theoretical analysis showing that TPC induces a quadratic, trajectory-coupled regularization that provably reduces gradient variance while preserving the underlying flow-matching objective. Instantiated within flow matching, TPC improves sample quality and efficiency across CIFAR-10 and ImageNet at multiple resolutions, achieving lower FID at identical or lower computational cost than prior methods, and extends seamlessly to modern SOTA-style pipelines with noise-augmented training, score-based denoising, and rectified flow.

## 1. Introduction

Continuous-time generative models have become a popular framework for high-fidelity image synthesis, encompassing both diffusion models (DMs) and deterministic continuous normalizing flows (NFs). DMs have achieved state-of-the-art performance across a wide range of benchmarks, benefiting from stable training objectives and well-understood stochastic dynamics (Ho et al., 2020; Rombach et al., 2022; Yang et al., 2023), but are often at the cost of long sampling

<sup>1</sup>William & Mary. Correspondence to: Jindong Wang <jdw@wm.edu>.

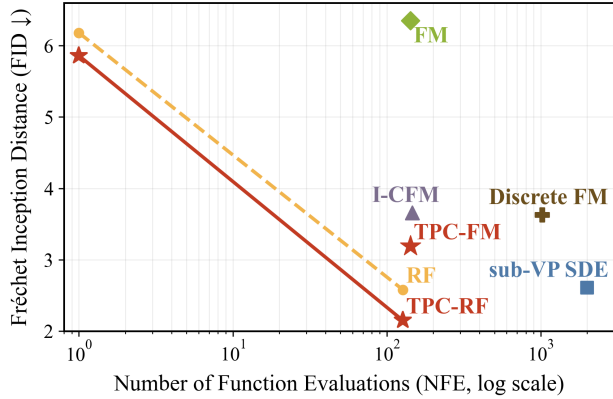


**Figure 1. Sample quality vs. sampling efficiency.** Fréchet Inception Distance (FID  $\downarrow$ ) versus number of function evaluations (NFE, log scale) on CIFAR-10. Temporal Pair Consistency (TPC) consistently shifts the quality–efficiency frontier by suppressing temporal oscillations in the learned vector field, achieving lower FID at identical or lower computational cost without modifying the underlying model or solver.

trajectories and substantial computational overhead. In parallel, recent work has revisited deterministic formulations based on ordinary differential equations, demonstrating that carefully designed probability paths—such as those used in flow matching (FM) (Lipman et al., 2023) and rectified flow (Liu et al., 2023)—can offer greater flexibility and improved sampling efficiency while retaining competitive generation quality (Li et al., 2023).

Despite recent progress, existing flow-matching-based generative models still exhibit important limitations in how temporal dynamics are learned. Standard flow matching trains the velocity field as a function of state and time, but does so independently at each time step, without explicitly constraining predictions across nearby times (Lipman et al., 2023; Liu et al., 2023). Intuitively, this independence wastes temporal correlation already present along each probability path: gradients at different timesteps share randomness but are treated as independent noise, inflating estimator variance (Boffi et al., 2025; Albergo & Vanden-Eijnden, 2023). Prior work has observed that this lack of temporal coherence induces curved trajectories in the marginal flow, which in turn lead to elevated gradient variance during training, as we also empirically observe (Figure 3), and

increased numerical error when coarse time discretizations are used at inference (Geng et al., 2025; Lee et al., 2025; Reu et al., 2025). In practice, this manifests as reduced sample efficiency: achieving high-quality samples requires finer discretization or a larger number of function evaluations, even when using identical solvers and probability paths (Esser et al., 2024). Figure 1 provides a direct manifestation of this effect: when the vector field is learned independently across time (FM, RF), identical sampling budgets yield substantially worse sample quality, whereas temporal pair consistency achieves markedly lower FID at the same number of function evaluations.

In this work, we introduce *Temporal Pair Consistency Flow Matching* (TPC-FM), a variance-reduced formulation of flow matching that explicitly enforces temporal coherence in the learned velocity field. Prior work on continuous-time generative models has explored temporal regularization through path-length penalties, Jacobian constraints, straight-trajectory objectives, or solver- and architecture-level design choices to improve stability and efficiency (Grathwohl et al., 2019a; Kidger, 2022; Liu et al., 2023; Ma et al., 2025; Geng et al., 2025). While effective, these approaches typically modify the function class, probability path, or inference procedure. TPC instead exploits a structural property of standard flow matching (Lipman et al., 2023): during training, velocity predictions at different timesteps along the *same* probability path are learned independently, despite being strongly correlated by construction. Directly enforcing temporal smoothness is nontrivial in this setting, since the target velocity field is defined only implicitly through stochastic path samples rather than an explicit time-continuous objective (Albergo & Vanden-Eijnden, 2023; Boffi et al., 2025). We show that this independence can be addressed by *pairing* timesteps sampled along the same path and encouraging consistency between their corresponding velocity predictions, yielding a lightweight, self-supervised regularization that operates entirely within the existing flow-matching objective. By coupling stochastic evaluations across time—without altering the probability path, neural architecture, or solver—TPC stabilizes optimization, substantially reduces training-time variance, and improves sample efficiency in practice, complementing recent advances in probability-path design and high-resolution flow-based generation (Esser et al., 2024; Ma et al., 2025; Zhai et al., 2025).

TPC-FM supports both simple and adaptive mechanisms for constructing temporal pairs. We show in Figure 3 that a fixed antithetic pairing strategy, which symmetrically couples early and late timesteps along the probability path, already yields substantial variance reduction, analogous to classical antithetic sampling in Monte Carlo estimation (Ren et al., 2019). To further adapt temporal coupling to the data and model, we additionally introduce a learnable

monotone pairing function that discovers effective temporal correspondences while preserving the ordered structure of the path. Temporal consistency is applied stochastically during training, ensuring that TPC-FM functions as a variance-reduction mechanism rather than a hard constraint. Because the formulation relies only on paired evaluations of the same probability path, it applies seamlessly to existing FM frameworks and remains compatible with recent deterministic path constructions such as rectified flow (Liu et al., 2023).

We evaluate TPC-FM across a spectrum of widely adopted image generation benchmarks that reflect both controlled analysis settings and modern high-resolution evaluation protocols. Specifically, we consider unconditional generation on CIFAR-10 (Krizhevsky & Hinton, 2009) and ImageNet (Krizhevsky et al., 2012) at resolutions up to  $128 \times 128$ , which remain the standard benchmarks for assessing optimization behavior, sample efficiency, and likelihood-quality trade-offs in continuous-time generative models, including recent diffusion and flow-matching frameworks (Karras et al., 2022; Yang et al., 2025; Ifriqi et al., 2025; Zhai et al., 2025). To assess practical relevance at modern resolutions, we further evaluate TPC-FM under noise-augmented training with score-based denoising on conditional ImageNet-64 and ImageNet-128, following the evaluation protocols used by recent state-of-the-art diffusion (Karras et al., 2022) and flow-based models (Zhai et al., 2025). Across diffusion-based, flow-matching, and rectified-flow formulations, TPC-FM consistently improves sample quality and sampling efficiency without introducing additional architectural complexity or inference cost. In the rectified-flow setting, temporal pair consistency complements trajectory straightening, yielding improved performance under both one-step and full-simulation regimes. Ablation studies further demonstrate that these gains are robust across pairing strategies and hyperparameter choices, confirming temporal coherence as a key factor in stabilizing and accelerating flow-based generative modeling.

**Contributions.** Our contributions are threefold:

- (i) We introduce *Temporal Pair Consistency* (TPC), a general variance-reduction principle for flow matching that enforces temporal coherence in the learned velocity field by coupling stochastic evaluations across time along the same probability path. TPC operates entirely within the standard flow-matching objective, without modifying probability paths, solvers, or model architectures. We provide a theoretical analysis that formalizes TPC as a quadratic, trajectory-coupled regularizer and establishes contraction and variance-reduction guarantees.
- (ii) We present practical instantiations of TPC using both *fixed* and *learnable* timestep pairing mechanisms, and show that temporal coupling can be incorporated without altering the underlying training loss or sampling

procedure. We further empirically demonstrate that TPC substantially reduces training-time variance in the learned vector field, by coupling temporally correlated gradients.

(iii) We demonstrate that TPC consistently improves sample quality and sampling efficiency across multiple continuous-time generative frameworks, including flow matching and rectified flow, on widely adopted image generation benchmarks. In particular, TPC yields gains under both standard probability-flow sampling and modern SOTA-style pipelines with noise-augmented training and score-based denoising.

## 2. Related Work

**Temporal and trajectory regularization in continuous-time models.** TPC is related at a high level to prior work on temporal smoothness, consistency regularization, and trajectory regularization in continuous-time generative models. Several approaches explicitly regularize the dynamics of learned ODEs by penalizing path length, kinetic energy, or Jacobians of the velocity field, often to improve numerical stability or invertibility in continuous normalizing flows (Chen et al., 2018; Grathwohl et al., 2019b; Kidger, 2022; Yang et al., 2025). Related ideas appear in diffusion models, where smoothness of the score or drift over time is implicitly encouraged through architectural design or discretization choices (Song et al., 2021b; Karras et al., 2022), as well as in recent work that explores straight-trajectory learning through latent-augmented or variational formulations of flow matching (Ma et al., 2025).

However, there are several important distinctions. First, TPC does not impose an explicit smoothness constraint on the velocity field with respect to time, nor does it regularize Jacobians or higher-order derivatives of the learned dynamics, unlike path- or Jacobian-based regularization methods (Grathwohl et al., 2019b; Kidger, 2022). Instead, it operates directly on paired stochastic evaluations of the flow-matching objective (Lipman et al., 2023), coupling velocity predictions at two timesteps sampled along the same probability path. As a result, TPC primarily targets the variance of the stochastic gradient estimator, rather than imposing a deterministic regularizer on the learned dynamics or function class.

**Consistency regularization.** TPC is also superficially related to consistency regularization techniques widely used in supervised and self-supervised learning, where model predictions are encouraged to be invariant under perturbations or augmentations (Laine & Aila, 2017; Sohn et al., 2020). Recent work has extended this idea to generative modeling through consistency models, which enforce output-level agreement across noise levels to enable one-step genera-

tion (Lu & Song, 2025; Issenhuth et al., 2024). In contrast, TPC does not enforce invariance of model outputs or define a fixed-point mapping across time; instead, it couples stochastic evaluations of the existing flow-matching objective to reduce estimator variance during training, while preserving the underlying continuous-time dynamics.

**Relation to flow matching and rectified flow.** Finally, TPC is complementary to recent advances in designing efficient probability paths for continuous-time generative modeling, including flow matching (Lipman et al., 2023), rectified flow (Liu et al., 2023), and temporally structured or expansive flow constructions (Ifriqi et al., 2025). While these methods focus on the choice of probability paths and the geometry of trajectories, TPC addresses a different aspect: the temporal structure of the training objective itself. Because TPC relies only on paired evaluations of the existing path sampler, it applies seamlessly to different probability paths and formulations, including both flow matching and rectified flow, without modifying the underlying generative model, solver, or sampling procedure. These distinctions position TPC as a lightweight and general mechanism for improving optimization stability and sample efficiency, rather than as an alternative probability path or solver design.

## 3. Method

Flow matching learns a time-indexed vector field that transports a simple reference distribution into the target data distribution by integrating an ordinary differential equation. In this section, we introduce *Temporal Pair Consistency Flow Matching* (TPC-FM), a variance-reduced formulation of flow matching that enforces temporal coherence between velocity predictions at paired timesteps. *Importantly*, TPC does not impose an explicit smoothness or Jacobian penalty on the velocity field; instead, it reduces stochastic gradient variance by coupling paired evaluations of the existing flow-matching objective. The key idea is to couple training examples across time in order to stabilize gradient estimates, improve sample efficiency, and reduce the mismatch between adjacent predictions of the velocity field. We begin by revisiting the flow-matching formulation 3.1, then introduce temporal pairs 3.2, describe fixed and learnable pairing mechanisms 3.3, offer theoretical insights 3.5, and conclude with the full training objective 3.6.

### 3.1. Conditional Flow Matching

Let  $x_0 \sim p_0$  denote a base distribution (e.g.,  $\mathcal{N}(0, I)$ ) and  $x_1 \sim p_1$  the data distribution. A probability path  $\{p_t\}_{t \in [0, 1]}$  is induced by a conditional map  $x_t = \Phi_t(x_0, x_1)$ , with associated velocity  $u_t(x_t) = \partial_t \Phi_t(x_0, x_1)$ . Flow matching parameterizes a velocity field  $v_\theta(x, t)$  and minimizes

$$\mathcal{L}_{\text{FM}}(\theta) = \mathbb{E}_{t \sim \rho, (x_0, x_1)} \|v_\theta(x_t, t) - u_t(x_t)\|_2^2, \quad (1)$$

where  $\rho$  is typically uniform on  $[0, 1]$ . Eq. (1) performs independent  $L^2(p_t)$  regressions across  $t$ , with no coupling between  $v_\theta(\cdot, t)$  and  $v_\theta(\cdot, t')$ .

### 3.2. Temporal Pairing for Variance Reduction

Temporal Pair Consistency (TPC) reduces variance in flow matching by coupling stochastic evaluations at two timesteps sampled along the same probability path. **Intuition.** In standard flow matching (Lipman et al., 2023), velocity predictions at different timesteps are trained independently, even when they lie on the same probability path and share endpoint randomness. As a result, the corresponding stochastic gradients are strongly correlated but treated as independent noise, leading to unnecessarily high estimator variance (Figure 3). TPC exploits this shared randomness by pairing timesteps and enforcing consistency between their velocity predictions, effectively yielding a control-variate estimator that cancels temporal noise while preserving the original objective.

Formally, for  $t \sim \rho$ , let  $t' = \psi(t)$  and draw a common endpoint pair  $(x_0, x_1)$ . The induced flow-matching states  $(x_t, u_t) = \mathcal{P}(x_0, x_1, t)$  and  $(x_{t'}, u_{t'}) = \mathcal{P}(x_0, x_1, t')$  yield velocity predictions  $v_t = v_\theta(x_t, t)$  and  $v_{t'} = v_\theta(x_{t'}, t')$ . Standard flow matching minimizes  $\mathbb{E}\|v_t - u_t\|_2^2$  independently across  $t$ . TPC instead augments this objective with a paired estimator

$$\ell_{\text{TPC}}(t, t') = \|v_t - u_t\|_2^2 + \|v_{t'} - u_{t'}\|_2^2 + \lambda\|v_t - v_{t'}\|_2^2,$$

which explicitly couples evaluations across time while preserving the underlying probability path and solver. By increasing correlation between paired gradient estimates through shared endpoint randomness  $(x_0, x_1)$ , this construction yields strict variance reduction via a control-variate effect and induces early collapse of training variance. Algorithm 1 describes practical implementations, including fixed and learned pairing rules and stochastic gating.

### 3.3. Pairing Mechanisms

Temporal Pair Consistency is defined by a pairing operator  $\psi : [0, 1] \rightarrow [0, 1]$  mapping a primary timestep  $t \sim \rho$  to an auxiliary timestep  $t' = \psi(t)$ . Given shared endpoints  $(x_0, x_1)$ , pairing induces coupled flow-matching states  $(x_t, u_t) = \mathcal{P}(x_0, x_1, t)$  and  $(x_{t'}, u_{t'}) = \mathcal{P}(x_0, x_1, t')$ , whose joint evaluation increases correlation between stochastic gradients and enables variance reduction.

**Fixed antithetic pairing.** A canonical choice is the antithetic map  $\psi_{\text{fix}}(t) = 1 - t$ , which pairs early and late times along the same probability path. For commonly used symmetric interpolants  $\Phi_t$  (e.g., linear or affine paths), the joint law of  $(x_t, x_{1-t})$  exhibits time-reversal symmetry (Lipman et al., 2023), making  $(t, 1 - t)$  an antithetic pair in the

sense of classical Monte Carlo variance reduction (Ren et al., 2019). As a result, the paired gradients  $g(t, \xi)$  and  $g(1-t, \xi)$  tend to be negatively correlated, yielding reduced estimator variance without introducing additional parameters.

**Learned monotone pairing.** To allow adaptive pairings beyond a fixed symmetry, we introduce a learnable map  $\phi : [0, 1] \rightarrow [0, 1]$  with  $t' = \phi(t)$  and impose the structural constraint  $\phi'(t) \geq 0$  to preserve temporal order. We parameterize  $\phi$  as  $\phi(t) = \sigma(\sum_{i=1}^H a_i \sigma(t + b_i) + c)$ , where  $\sigma$  denotes the sigmoid,  $a_i = \text{softplus}(\tilde{a}_i) > 0$  ensures nonnegative slope contributions,  $b_i \in \mathbb{R}$  control transition locations, and  $c \in \mathbb{R}$  sets a global offset. A single hidden layer suffices to approximate any monotone function on  $[0, 1]$  while keeping  $\phi$  low-capacity, consistent with its role as a structural estimator component rather than a predictive model.

Monotonicity is weakly enforced during optimization by penalizing order violations on a grid  $\{g_k = k/K\}_{k=1}^K$ , via  $r(\phi) = \sum_{k=1}^{K-1} \mathbf{1}\{\phi(g_{k+1}) < \phi(g_k)\}$ , where  $\mathbf{1}\{\cdot\}$  denotes the indicator function and  $K$  is a small constant ( $K = 32$ ). This regularizer biases  $\phi$  toward monotone solutions while retaining sufficient flexibility for data-dependent pairing. Both  $\psi_{\text{fix}}$  and  $\phi$  are implemented within the same paired estimator and training loop (Algorithm 1).

### 3.4. Temporal Consistency Objective

Temporal Pair Consistency augments the conditional flow-matching risk by introducing a quadratic coupling between velocity evaluations at paired times along a shared probability path. Let  $t \sim \rho$ ,  $t' = \psi(t)$ , and  $(x_t, u_t), (x_{t'}, u_{t'}) = \mathcal{P}(x_0, x_1, t), (x_0, x_1, t')$  denote path-sampled states with predictions  $v_t = v_\theta(x_t, t)$  and  $v_{t'} = v_\theta(x_{t'}, t')$ . The temporal consistency penalty is defined pointwise as  $\ell_{\text{TPC}}(t, t') := \|v_t - v_{t'}\|_2^2$ , which enforces coherence of  $v_\theta$  across paired evaluations sharing the same endpoint randomness  $(x_0, x_1)$ .

For a single sample, the resulting objective takes the form

$$\mathcal{L}(\theta) = \|v_t - u_t\|_2^2 + \lambda_{\text{tpc}}\|v_t - v_{t'}\|_2^2 + \lambda_{\text{mono}}r(\phi),$$

where  $\lambda_{\text{tpc}}, \lambda_{\text{mono}} \geq 0$ . At the population level, this corresponds to minimizing a Tikhonov-regularized risk  $\mathbb{E}_{t, (x_0, x_1)}\|v_\theta(x_t, t) - u_t\|_2^2 + \lambda_{\text{tpc}}\mathbb{E}_{t, t'}\|v_\theta(x_t, t) - v_\theta(x_{t'}, t')\|_2^2$ , which selects, among near-minimizers of the unregularized flow-matching objective, velocity fields with reduced temporal oscillation along path-coupled states.

From an optimization perspective, the paired term induces correlation between stochastic gradients  $g(t, \xi) = \nabla_\theta\|v_t - u_t\|_2^2$  and  $g(t', \xi) = \nabla_\theta\|v_{t'} - u_{t'}\|_2^2$  under shared randomness  $\xi = (x_0, x_1)$ , yielding a control-variate effect and strict variance reduction. This coupling operates entirely at the

estimator level and preserves the underlying conditional flow-matching formulation, as formalized in Section 3.5.

**Stochastic gating.** To avoid over-regularization and ensure that temporal coupling functions as a variance-reduction mechanism rather than a dominant bias, we apply TPC through a gated estimator. Let  $b \sim \text{Bernoulli}(p_{\text{tpc}})$  and define the gated loss  $\tilde{\ell}_{\text{TPC}}(t, t') = b \ell_{\text{TPC}}(t, t')$ . The resulting objective satisfies  $\mathbb{E}[\ell_{\text{TPC}}] = p_{\text{tpc}} \ell_{\text{TPC}}$  while preserving stochastic exposure to the unregularized flow-matching gradient. This randomized coupling stabilizes optimization, induces early variance collapse, and maintains expressive flexibility of the learned velocity field. Algorithm 1 summarizes the complete training procedure.

### 3.5. Theoretical Analysis

The following analysis (Appendix A) formalizes the intuition (Section 3.2), showing that temporal pairing induces a control-variate estimator with strictly reduced gradient variance.

**TPC as a regularized population objective.** Let  $x_t = \Phi_t(x_0, x_1)$  be the path-sampled state and  $u_t(x_0, x_1)$  the conditional FM target. Standard FM minimizes  $\mathcal{R}(v) = \mathbb{E}\|v(x_t, t) - u_t\|_2^2$ , whose population minimizer is the conditional expectation (an  $L^2$  projection). TPC augments FM with the coupled penalty  $\|v\|_{\text{TPC}}^2 = \mathbb{E}\|v(x_t, t) - v(x_{t'}, t')\|_2^2$  for paired  $t' = \psi(t)$ , yielding  $\mathcal{R}_\lambda(v) = \mathcal{R}(v) + \lambda\|v\|_{\text{TPC}}^2$ . This is a Tikhonov-regularized risk that selects, among near-minimal FM solutions, predictors with reduced temporal oscillation along path-coupled states and satisfies the deterministic contraction bound  $\|v_\lambda\|_{\text{TPC}}^2 \leq \mathcal{R}(v^*)/\lambda$  for any  $v_\lambda \in \arg \min \mathcal{R}_\lambda$ .

**Optimization: strict variance reduction via coupling.** For the per-sample FM gradient  $g(t, \xi) = \nabla_\theta \|v_\theta(x_t, t) - u_t\|_2^2$  (with shared randomness  $\xi$  generating  $(x_0, x_1)$ ), temporal pairing induces a control-variate estimator  $g(t, \xi) - \alpha g(t', \xi)$ . Under mild regularity that implies nontrivial positive correlation between paired gradients, the optimal  $\alpha^*$  yields the standard strict reduction  $\text{Var}(g - \alpha^* g') = \text{Var}(g)(1 - \rho^2)$ , where  $\rho = \text{Corr}(g, g')$ . TPC increases this correlation by explicitly enforcing coherence of  $v_\theta$  across paired times, thereby reducing gradient noise.

**Sampling: improved probability-flow numerics.** Generation integrates the probability-flow ODE  $\dot{z}_t = v_\theta(z_t, t)$ . Classical discretization bounds depend not only on Lipschitzness in  $x$  but also on temporal variation of the vector field. Because  $\|v_\theta\|_{\text{TPC}}$  penalizes temporal roughness along states visited by the path sampler (and locally approximates a time-derivative seminorm), TPC reduces effective time-variation on-trajectory, improving numerical stability

at fixed step size (or reducing the required NFE for a target error).

These results certify TPC as a principled mechanism—simultaneously estimator-theoretic (variance reduction), functional-analytic (temporal regularization), and numerical (ODE stability)—that explains the empirical improvements observed for flow matching.

### 3.6. Full Training Objective

The complete training procedure combines conditional flow matching, stochastic temporal pairing, and monotonicity regularization (Algorithm 1). For  $t \sim \rho$ ,  $t' = \psi(t)$ , and  $b \sim \text{Bernoulli}(p_{\text{tpc}})$ , the TPC–FM estimator minimizes the joint expectation

$$\mathbb{E} \left[ \|v_\theta(x_t, t) - u_t\|_2^2 + b \lambda_{\text{tpc}} \|v_\theta(x_t, t) - v_\theta(x_{t'}, t')\|_2^2 \right. \\ \left. + \lambda_{\text{mono}} r(\phi) \right]. \quad (2)$$

where  $(x_t, u_t), (x_{t'}, u_{t'}) = \mathcal{P}(x_0, x_1, t), (x_0, x_1, t')$  are path-sampled states. The first term recovers standard flow matching, while the remaining terms introduce randomized quadratic coupling across paired timesteps and enforce monotonic structure on the pairing map  $\phi$ .

Gradients w.r.t.  $\theta$  arise from both flow-matching and temporal-consistency terms, while  $\phi$  is optimized via the paired consistency loss and monotonicity regularization. Because the objective depends only on paired evaluations of the path sampler  $\mathcal{P}$ , it applies unchanged to deterministic or stochastic, continuous or discretized probability paths.

## 4. Experiments

### 4.1. Setup

We evaluate on standard unconditional image generation benchmarks following established protocols in diffusion and continuous-time generative modeling (Ho et al., 2020; Song et al., 2021b; Lipman et al., 2023; Liu et al., 2023), comparing against state-of-the-art diffusion- and flow-based models reported on these benchmarks (Dhariwal & Nichol, 2021; Karras et al., 2022). Experiments are conducted on CIFAR-10 and ImageNet at resolutions  $32 \times 32$ ,  $64 \times 64$ , and  $128 \times 128$ , enabling direct comparison across diffusion, score-based, flow-matching, and rectified-flow methods. Unless otherwise stated, all models are unconditional and share the same U-Net backbone, architectural capacity, and training budget, ensuring that observed differences arise from the learning objective and probability path rather than model size or optimization artifacts. We report negative log-likelihood (NLL) where applicable, Fréchet Inception Distance (FID) for sample quality, and the number of function evaluations (NFE) as a measure of sampling efficiency. For flow-based models, samples are generated by solving the

---

**Algorithm 1** Flow Matching with Temporal Pair Consistency (TPC)

---

**Require:** Model  $f_\theta$ , path sampler  $\mathcal{P}$ , pairing function  $\phi$ , TPC probability  $p_{\text{tpc}}$ , weights  $\lambda_{\text{tpc}}, \lambda_{\text{mono}}$ .

- 1: **Monotone pairing function:**
- 2:  $\phi(t) = \sigma\left(\sum_{i=1}^H a_i \sigma(t + b_i) + c\right)$ , where  $a_i = \text{softplus}(\tilde{a}_i) > 0$ .
- 3: **Fixed pairing:**  $t'_{\text{fixed}} = 1 - t$
- 4: **Learned pairing:**  $t'_{\text{learned}} = \phi(t)$
- 5: **for** each minibatch  $(x_1)$  **do**
- 6:   Sample  $x_0$  and  $t \sim \mathcal{U}(0, 1)$
- 7:    $(x_t, u_t) = \mathcal{P}(x_0, x_1, t)$
- 8:    $v_t = f_\theta(x_t, t)$
- 9:    $\mathcal{L}_{\text{FM}} = \|v_t - u_t\|^2$
- 10:   Sample  $b \sim \text{Bernoulli}(p_{\text{tpc}})$
- 11:   **if**  $b = 1$  **then**
- 12:     **if** fixed pairing **then**
- 13:        $t' = t'_{\text{fixed}}$
- 14:     **else**
- 15:        $t' = t'_{\text{learned}}$
- 16:     **end if**
- 17:      $(x_{t'}, u_{t'}) = \mathcal{P}(x_0, x_1, t')$
- 18:      $v_{t'} = f_\theta(x_{t'}, t')$
- 19:      $\mathcal{L}_{\text{TPC}} = \|v_t - v_{t'}\|^2$
- 20:   **else**
- 21:      $\mathcal{L}_{\text{TPC}} = 0$
- 22:   **end if**
- 23:   Construct grid  $g_1, \dots, g_K$
- 24:    $r(\phi) = \sum_{i=1}^{K-1} \mathbf{1}[\phi(g_{i+1}) < \phi(g_i)]$
- 25:    $\mathcal{L} = \mathcal{L}_{\text{FM}} + \lambda_{\text{tpc}} \mathcal{L}_{\text{TPC}} + \lambda_{\text{mono}} r(\phi)$
- 26:   Update  $\theta, \phi$  by SGD
- 27: **end for**
- 28: **return**  $f_\theta, \phi$

---

learned generative ODE from noise to data: Flow Matching models use adaptive ODE solvers with absolute and relative tolerances set to  $10^{-5}$  (Lipman et al., 2023), while Rectified Flow models use adaptive Runge–Kutta (RK45) solvers for full simulation and fixed-step Euler solvers for few-step, one-step, and distillation settings (Liu et al., 2023). All FID, IS, and recall metrics are computed using standard evaluation protocols over 50k samples. To isolate the effect of temporal structure, we ablate the temporal prior probability  $p_{\text{tpc}}$ , transition strength  $\lambda_{\text{tpc}}$ , and monotonicity regularization weight  $\lambda_{\text{mono}}$ , considering both fixed and learned pairing mechanisms; hyperparameters are selected on held-out validation sets, fixed across datasets, and evaluated across ODE, SDE, and rectified-flow formulations under both one-step and full-simulation regimes. For ImageNet experiments targeting modern SOTA regimes, we additionally evaluate noise-augmented flow matching with score-based denoising at sampling time, following high-

resolution generative pipelines used in prior work (Dhariwal & Nichol, 2021; Song et al., 2021b; Karras et al., 2022), using identical noise configurations for baseline FM and TPC-FM unless otherwise stated to ensure controlled comparisons.

## 4.2. Unconditional Image Generation

**Flow Matching** Table 1 reports unconditional image generation results on CIFAR-10 and ImageNet at resolutions  $32 \times 32$ ,  $64 \times 64$ , and  $128 \times 128$ . Across all datasets and resolutions, TPC-FM consistently improves upon prior flow-matching objectives, achieving lower FID at identical or lower NFE while maintaining competitive likelihoods. On CIFAR-10, TPC-FM reduces FID from 6.35 (FM w/ OT) to 3.19 at the same NFE, matching the best reported NLL among flow-based methods. Similar gains are observed on ImageNet  $32 \times 32$  and  $64 \times 64$ , where TPC-FM attains the lowest FID among all compared diffusion and flow-matching models without increased sampling cost. At higher resolution, TPC-FM continues to scale favorably, improving FID on ImageNet  $128 \times 128$  from 20.9 to 18.6 while matching likelihood performance. Notably, these improvements are achieved without additional sampling steps or architectural changes, indicating that temporal pair consistency improves the learned probability paths rather than relying on increased numerical resolution.

**Rectified Flow** Table 2 reports results for rectified flow (RF), probability-flow ODEs, and SDE baselines under one-step and full-simulation regimes. Consistent with prior work (Liu et al., 2023), rectified flows outperform probability-flow ODEs in the one-step setting and achieve competitive quality–efficiency trade-offs under full simulation. Across all rectification depths, applying temporal pair consistency (TPC-RF) yields consistent improvements in FID and recall at identical NFE, both for single-step generation and adaptive Runge–Kutta simulation. For example, TPC-2RF improves one-step FID from 4.85 to 4.55 while increasing recall, and under full simulation reduces FID from 2.58 to 2.15 without additional function evaluations. These gains indicate that temporal pair consistency improves the quality of the learned vector field itself, complementing rectification without relying on increased solver depth or numerical resolution.

## 4.3. Extending TPC to Modern SOTA-Style Flow

While the preceding sections demonstrate that TPC improves standard flow matching under probability–flow sampling, this regime alone does not reflect how state-of-the-art generative models are trained and evaluated at modern resolutions. In practice, competitive ImageNet performance relies on *noise-augmented training with score-based denoising at sampling time*, a design shared by modern diffusion

Table 1. Diffusion and Flow-Matching Results on CIFAR-10, ImageNet 32×32, ImageNet 64×64, and ImageNet 128×128. Blank entries indicate methods that do not report unconditional ImageNet results and are evaluated primarily under guided or SOTA-style training; see Tables 3 and 4 for matched comparisons.

Model	CIFAR-10			ImageNet 32×32			ImageNet 64×64		
	NLL↓	FID↓	NFE↓	NLL↓	FID↓	NFE↓	NLL↓	FID↓	NFE↓
DDPM (Ho et al., 2020)	3.12	7.48	274	3.54	6.99	262	3.32	17.36	264
Score Matching (Lipman et al., 2023)	3.16	19.94	242	3.56	5.68	178	3.40	19.74	441
i-DODE (Zheng et al., 2023b)	2.56	11.20	162	3.69	10.31	138	—	—	—
ScoreFlow (Lipman et al., 2023)	3.09	20.78	428	3.55	14.14	195	3.36	24.95	601
FM w/ Diffusion (Lipman et al., 2023)	3.10	8.06	183	3.54	6.37	193	3.33	16.88	187
FM w/ OT (Lipman et al., 2023)	2.99	6.35	142	3.53	5.02	122	3.31	14.45	138
I-CFM (Tong et al., 2024)	—	3.66	146	—	—	—	—	—	—
OT-CFM (Tong et al., 2024)	—	3.58	134	—	—	—	—	—	—
Discrete FM (Gat et al., 2024)	—	3.63	1024	—	—	—	—	—	—
V-RFM (Guo & Schwing, 2025)	—	3.58	1000	—	—	—	—	—	—
<b>TPC-FM (Ours)</b>	<b>2.99</b>	<b>3.19</b>	<b>142</b>	<b>3.53</b>	<b>4.22</b>	<b>122</b>	<b>3.31</b>	<b>13.14</b>	<b>138</b>

Table 2. Benchmarking TPC on RF, SDE, ODE Methods.

Method	NFE (↓)	IS (↑)	FID (↓)	Recall (↑)
<i>One-Step Generation + Distil (Euler solver, N=1)</i>				
1-Rectified Flow	1	9.08	6.18	0.45
2-Rectified Flow	1	9.01	4.85	0.50
3-Rectified Flow	1	8.79	5.21	0.51
VP ODE	1	8.73	16.23	0.29
sub-VP ODE	1	8.80	14.32	0.35
<i>Full Simulation (Runge–Kutta RK45), Adaptive N</i>				
1-Rectified Flow	127	9.60	2.58	0.57
2-Rectified Flow	110	9.24	3.36	0.54
3-Rectified Flow	104	9.01	3.96	0.53
VP ODE	140	9.37	3.93	0.51
sub-VP ODE	146	9.46	3.16	0.55
<i>Full Simulation (Euler solver, N=2000)</i>				
VP SDE	2000	9.58	2.55	0.58
sub-VP SDE	2000	9.56	2.61	0.58
<i>One-Step Generation + Distil (Euler solver, N=1)</i>				
<b>TPC-1RF (ours)</b>	<b>1</b>	<b>9.21</b>	<b>5.86</b>	<b>0.47</b>
<b>TPC-2RF (ours)</b>	<b>1</b>	<b>9.14</b>	<b>4.55</b>	<b>0.53</b>
<b>TPC-3RF (ours)</b>	<b>1</b>	<b>8.92</b>	<b>4.83</b>	<b>0.53</b>
<i>Full Simulation (Runge–Kutta RK45), Adaptive N</i>				
<b>TPC-1RF (ours)</b>	<b>127</b>	<b>9.78</b>	<b>2.15</b>	<b>0.6</b>
<b>TPC-2RF (ours)</b>	<b>110</b>	<b>9.42</b>	<b>2.95</b>	<b>0.58</b>
<b>TPC-3RF (ours)</b>	<b>104</b>	<b>9.18</b>	<b>3.45</b>	<b>0.55</b>

and flow-based models (Dhariwal & Nichol, 2021; Song et al., 2021b; Zhai et al., 2025). As a result, gains under clean probability–flow sampling do not fully characterize practical performance at scale.

We therefore evaluate TPC as an *orthogonal training principle* under noise-augmented flow matching with score-based denoising, preserving the underlying flow-matching objective while matching modern SOTA evaluation protocols (Zhai et al., 2025). As in prior work, denoising is performed using the model-implied score of the noise-augmented probability flow, ensuring that improvements arise from the learned flow field rather than post-processing

Model (IN 128 × 128)	NLL↓	FID↓
MGAN (Hoang et al., 2018)	—	58.9
PacGAN2 (Lin et al., 2018)	—	57.5
Logo-GAN-AE (Sage et al., 2018)	—	50.9
Self-cond. GAN (Lucić et al., 2019)	—	41.7
Uncond. BigGAN (Lucić et al., 2019)	—	25.3
PGMGAN (Armandpour et al., 2021)	—	21.7
FM w/ OT (Lipman et al., 2023)	2.90	20.9
<b>TPC-FM (Ours)</b>	<b>2.90</b>	<b>18.6</b>

Table 3. Conditional ImageNet 128 × 128 generation performance (FID ↓). All methods are evaluated under noise-augmented training with score-based denoising at sampling time.

Model	Model Class	FID ↓
ADM-G (Dhariwal & Nichol, 2021)	Diff/ FM	2.97
CDM (Ho et al., 2022)	Diff/ FM	3.52
Simple Diffusion (Hoogeboom et al., 2023)	Diff/ FM	1.94
RIN (Jabri et al., 2023)	Diff/ FM	2.75
BigGAN (Brock et al., 2019)	GAN	8.70
BigGAN-deep (Brock et al., 2019)	GAN	5.70
TARFLOW ( $\sigma = 0.05$ ) (Zhai et al., 2025)	NF	5.29
TARFLOW ( $\sigma = 0.15$ ) (Zhai et al., 2025)	NF	5.03
FM + noise + denoising (baseline)	FM	6.8
<b>TPC-FM + noise + denoising (ours)</b>	<b>FM</b>	<b>4.9</b>

heuristics.

We evaluate this setting on conditional ImageNet generation at  $64 \times 64$  and  $128 \times 128$ , comparing TPC-FM against diffusion (Dhariwal & Nichol, 2021; Nichol & Dhariwal, 2021), GAN (Brock et al., 2019), normalizing-flow (Zhai et al., 2025), and flow-matching baselines under identical noise-augmented and denoised protocols (Tables 4 and 3).

**Noise specification.** In all SOTA-style evaluations, we adopt additive Gaussian noise during training to match modern high-resolution flow-based pipelines (Song et al., 2021b; Zhai et al., 2025). Specifically, states along the probability path are perturbed as  $x_t \leftarrow x_t + \varepsilon$ , with  $\varepsilon \sim \mathcal{N}(0, \sigma^2 I)$ . The noise scale  $\sigma$  is selected to balance denoising strength and flow fidelity and is chosen *exclusively* to optimize FID under the baseline flow-matching setup. Unless otherwise stated, we use  $\sigma = 0.05$  for ImageNet-64 and  $\sigma = 0.15$  for ImageNet-128. These values are then held fixed when training TPC-FM, with no additional tuning, ensuring that all improvements are attributable to temporal pair consistency rather than noise hyperparameter selection.

**Table 4.** Conditional ImageNet  $64 \times 64$  generation performance (FID  $\downarrow$ ). All methods are evaluated under noise-augmented training with score-based denoising at sampling time.

Model	Model Class	FID $\downarrow$
EDM (Karras et al., 2022)	Diff/FM	1.55
iDDPM (Nichol & Dhariwal, 2021)	Diff/FM	2.92
ADM (dropout) (Dhariwal & Nichol, 2021)	Diff/FM	2.09
IC-GAN (Casanova et al., 2021)	GAN	6.70
BigGAN (Brock et al., 2019)	GAN	4.06
CD (LPIPS) (Song et al., 2023)	CM	4.70
iCT-deep (Song & Dhariwal, 2024)	CM	3.25
TARFLOW [4-1024-8-8- $\mathcal{N}(0, 0.05^2)$ ] (Zhai et al., 2025)	NF	3.99
TARFLOW [2-768-8-8- $\mathcal{N}(0, 0.05^2)$ ] (Zhai et al., 2025)	NF	2.90
TARFLOW [2-1024-8-8- $\mathcal{N}(0, 0.05^2)$ ] (Zhai et al., 2025)	NF	2.66
FM + noise + denoising (baseline)	FM	3.6
<b>TPC-FM + noise + denoising (ours)</b>	<b>FM</b>	<b>2.4</b>

**Table 5.** Fixed TPC-FM FID results across temporal prior probability  $p_{\text{tpc}}$  and transition strength  $\lambda_{\text{tpc}}$ .

$p_{\text{tpc}}$	$\lambda_{\text{tpc}}$				Best
	0.1	0.25	0.5	1.0	
0.25	3.895	3.833	4.104	4.314	3.833
0.50	5.101	4.794	4.756	4.216	4.216
0.75	4.089	4.101	4.075	3.931	3.931
1.00	4.309	<b>3.594</b>	4.179	6.545	<b>3.594</b>
			Baseline		6.35

#### 4.4. Ablation Studies

Tables 5–7 analyze the effects of the temporal prior probability  $p_{\text{tpc}}$ , transition strength  $\lambda_{\text{tpc}}$ , and monotonicity regularization  $\lambda_{\text{mono}}$  on CIFAR-10. Across all settings, TPC-FM consistently improves over the FM w/ OT baseline (FID 6.35), demonstrating robustness to hyperparameter choice. Moderate temporal coupling yields the best performance, while overly large  $\lambda_{\text{tpc}}$  degrades quality, indicating that excessive temporal constraints can restrict the learned probability path. Learning  $p_{\text{tpc}}$  further improves performance over fixed priors, achieving the best overall result at  $p_{\text{tpc}} = 0.75$ ,  $\lambda_{\text{tpc}} = 0.10$  (FID 3.19). Introducing a weak monotonicity regularizer consistently improves sample quality, with small  $\lambda_{\text{mono}}$  values yielding the lowest FID, while stronger regularization degrades performance. These results indicate that temporal pair consistency is effective under mild coupling and regularization, with learned pairing providing additional gains; representative qualitative samples are shown in Figure 2.

## 5. Conclusion

We introduced Temporal Pair Consistency (TPC), a lightweight variance-reduction principle with theoretical guarantees that enforces coherence between velocity predictions at paired timesteps along the same probability path. Applied to flow matching and rectified flow, TPC consis-

**Table 6.** Learned TPC-FM FID results across temporal prior probability  $p_{\text{tpc}}$  and transition strength  $\lambda_{\text{tpc}}$ .

$p_{\text{tpc}}$	$\lambda_{\text{tpc}}$				Best
	0.1	0.25	0.5	1.0	
0.25	3.922	4.249	4.767	4.513	3.922
0.50	3.895	3.885	4.266	4.723	3.885
0.75	<b>3.193</b>	3.620	4.016	3.898	<b>3.193</b>
1.00	4.402	4.382	4.914	6.223	4.382
			Baseline		6.35

**Table 7.** Effect of  $\lambda_{\text{mono}}$  on FID  $\downarrow$  for learned and fixed TPC.

$\lambda_{\text{mono}}$	0	0.001	0.005	0.010	0.020	0.050
<b>Learned</b>						
FID $\downarrow$	3.563	<b>3.193</b>	4.124	3.640	3.406	3.304
<b>Fixed</b>						
FID $\downarrow$	4.012	<b>3.594</b>	4.671	4.118	3.882	3.741

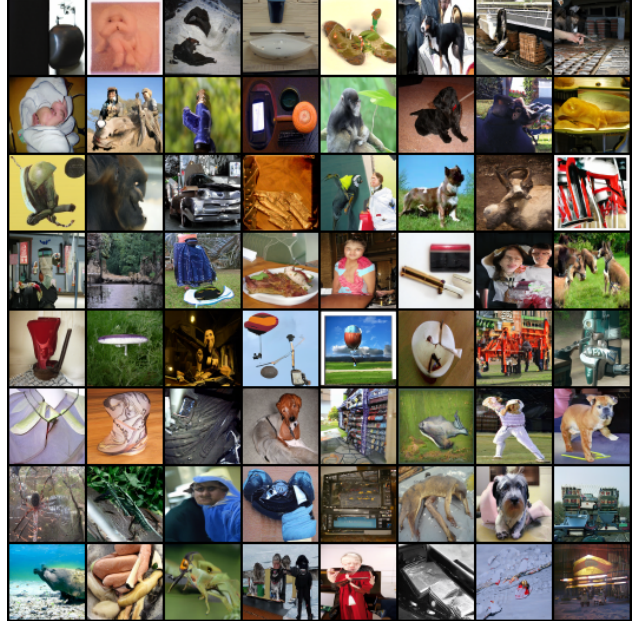


**Figure 2.** ImageNet Qualitative Samples.

tently improves sample quality and efficiency across one-step and full-simulation regimes and extends seamlessly to modern SOTA-style pipelines, demonstrating that simple temporal coupling can replace more complex path or solver designs.

**Limitations** This work focuses on unconditional image generation at resolutions up to  $128 \times 128$ . While we show that TPC remains effective under modern SOTA-style training pipelines, extending it to conditional settings, higher resolutions, and other modalities is left to future work.

## Acknowledgements

This work was partially supported by the Commonwealth Cyber Initiative (CCI) program (H-2Q25-020), the William & Mary Faculty Research Award, the Modal Academic Compute Award, and computational resources provided by the NSF ACCESS program under allocations CIS250827 and CIS251183, with support from the NCSA Delta and DeltaAI systems.

## Impact Statement

This paper presents work whose goal is to advance the field of Machine Learning. There are many potential societal consequences of our work, none which we feel must be specifically highlighted here.

## References

Albergo, M. S. and Vanden-Eijnden, E. Building normalizing flows with stochastic interpolants. In *The Eleventh International Conference on Learning Representations*, 2023. URL <https://openreview.net/forum?id=li7qeBbCR1t>.

Armandpour, M., Sadeghian, A., Li, C., and Zhou, M. Partition-Guided GANs . In *2021 IEEE/CVF Conference on Computer Vision and Pattern Recognition (CVPR)*, pp. 5095–5105, Los Alamitos, CA, USA, June 2021. IEEE Computer Society. doi: 10.1109/CVPR46437.2021.00506. URL <https://doi.ieee.org/10.1109/CVPR46437.2021.00506>.

Boffi, N. M., Albergo, M. S., and Vanden-Eijnden, E. Flow map matching with stochastic interpolants: A mathematical framework for consistency models. *Transactions on Machine Learning Research*, 2025. ISSN 2835-8856. URL <https://openreview.net/forum?id=cqDH0e6ak2>.

Brock, A., Donahue, J., and Simonyan, K. Large scale GAN training for high fidelity natural image synthesis. In *International Conference on Learning Representations*, 2019. URL <https://openreview.net/forum?id=B1xsqj09Fm>.

Casanova, A., Careil, M., Verbeek, J., Drozdzal, M., and Romero, A. Instance-conditioned GAN. In Beygelzimer, A., Dauphin, Y., Liang, P., and Vaughan, J. W. (eds.), *Advances in Neural Information Processing Systems*, 2021. URL [https://openreview.net/forum?id=aUuTEEcY\\_](https://openreview.net/forum?id=aUuTEEcY_).

Chen, R. T. Q., Rubanova, Y., Bettencourt, J., and Duvenaud, D. Neural ordinary differential equations. In *Proceedings of the 32nd International Conference on Neural Information Processing Systems*, NIPS’18, pp. 6572–6583, Red Hook, NY, USA, 2018. Curran Associates Inc.

Dhariwal, P. and Nichol, A. Q. Diffusion models beat GANs on image synthesis. In Beygelzimer, A., Dauphin, Y., Liang, P., and Vaughan, J. W. (eds.), *Advances in Neural Information Processing Systems*, 2021. URL <https://openreview.net/forum?id=AAWuCvzaVt>.

Esser, P., Kulal, S., Blattmann, A., Entezari, R., Müller, J., Saini, H., Levi, Y., Lorenz, D., Sauer, A., Boesel, F., Podell, D., Dockhorn, T., English, Z., and Rombach, R. Scaling rectified flow transformers for high-resolution image synthesis. In *Proceedings of the 41st International Conference on Machine Learning*, ICML’24. JMLR.org, 2024.

Gat, I., Remez, T., Shaul, N., Kreuk, F., Chen, R. T. Q., Synnaeve, G., Adi, Y., and Lipman, Y. Discrete flow matching. In Globerson, A., Mackey, L., Belgrave, D., Fan, A., Paquet, U., Tomczak, J., and Zhang, C. (eds.), *Advances in Neural Information Processing Systems*, volume 37, pp. 133345–133385. Curran Associates, Inc., 2024. doi: 10.5220/079017-4239. URL [https://proceedings.neurips.cc/paper\\_files/paper/2024/file/f0d629a734b56a642701bba7bc8bb3ed-Paper-Conference.pdf](https://proceedings.neurips.cc/paper_files/paper/2024/file/f0d629a734b56a642701bba7bc8bb3ed-Paper-Conference.pdf).

Geng, Z., Deng, M., Bai, X., Kolter, J. Z., and He, K. Mean flows for one-step generative modeling. In *The Thirty-ninth Annual Conference on Neural Information Processing Systems*, 2025. URL <https://openreview.net/forum?id=uWj4s7rMnR>.

Grathwohl, W., Chen, R. T. Q., Bettencourt, J., and Duvenaud, D. Scalable reversible generative models with free-form continuous dynamics. In *International Conference on Learning Representations*, 2019a. URL <https://openreview.net/forum?id=rJxgknCcK7>.

Grathwohl, W., Chen, R. T. Q., Bettencourt, J., Sutskever, I., and Duvenaud, D. FFJORD: free-form continuous dynamics for scalable reversible generative models. In *7th International Conference on Learning Representations, ICLR 2019, New Orleans, LA, USA, May 6-9, 2019*. Open-Review.net, 2019b. URL <https://openreview.net/forum?id=rJxgknCcK7>.

Guo, P. and Schwing, A. Variational rectified flow matching. In *Forty-second International Conference on Machine Learning*, 2025. URL <https://openreview.net/forum?id=Rk18ZikrFI>.

Ho, J., Jain, A., and Abbeel, P. Denoising diffusion probabilistic models. In Larochelle, H., Ranzato, M., He, H., Grauman, K., and亠, A. (eds.), *Advances in Neural Information Processing Systems*, NIPS’25, pp. 10000–10010, Red Hook, NY, USA, 2025. Curran Associates Inc.

M., Hadsell, R., Balcan, M., and Lin, H. (eds.), *Advances in Neural Information Processing Systems*, volume 33, pp. 6840–6851. Curran Associates, Inc., 2020. URL [https://proceedings.neurips.cc/paper\\_files/paper/2020/file/4c5bcfec8584af0d967f1ab10179ca4b-Paper.pdf](https://proceedings.neurips.cc/paper_files/paper/2020/file/4c5bcfec8584af0d967f1ab10179ca4b-Paper.pdf).

Ho, J., Saharia, C., Chan, W., Fleet, D. J., Norouzi, M., and Salimans, T. Cascaded diffusion models for high fidelity image generation. *J. Mach. Learn. Res.*, 23(1), January 2022. ISSN 1532-4435.

Hoang, Q., Nguyen, T. D., Le, T., and Phung, D. MGAN: Training generative adversarial nets with multiple generators. In *International Conference on Learning Representations*, 2018. URL <https://openreview.net/forum?id=rkmu5b0a->.

Hoogeboom, E., Heek, J., and Salimans, T. Simple diffusion: end-to-end diffusion for high resolution images. In *Proceedings of the 40th International Conference on Machine Learning*, ICML’23. JMLR.org, 2023.

Ifriqi, T. B., Nguyen, J., Alahari, K., Verbeek, J., and Chen, R. T. Q. Flowception: Temporally expansive flow matching for video generation, 2025. URL <https://arxiv.org/abs/2512.11438>.

Issenhuth, T., Santos, L. D., Franceschi, J.-Y., and Rakotomamonjy, A. Improving consistency models with generator-induced coupling. In *ICML 2024 Workshop on Structured Probabilistic Inference & Generative Modeling*, 2024. URL <https://openreview.net/forum?id=wt5ymd3h8h>.

Jabri, A., Fleet, D. J., and Chen, T. Scalable adaptive computation for iterative generation. In *Proceedings of the 40th International Conference on Machine Learning*, ICML’23. JMLR.org, 2023.

Jiang, Y., Chang, S., and Wang, Z. Transgan: Two pure transformers can make one strong gan, and that can scale up. In Ranzato, M., Beygelzimer, A., Dauphin, Y., Liang, P., and Vaughan, J. W. (eds.), *Advances in Neural Information Processing Systems*, volume 34, pp. 14745–14758. Curran Associates, Inc., 2021. URL [https://proceedings.neurips.cc/paper\\_files/paper/2021/file/7c220a2091c26a7f5e9f1cfb099511e3-Paper.pdf](https://proceedings.neurips.cc/paper_files/paper/2021/file/7c220a2091c26a7f5e9f1cfb099511e3-Paper.pdf).

Karras, T., Aittala, M., Aila, T., and Laine, S. Elucidating the design space of diffusion-based generative models. In Koyejo, S., Mohamed, S., Agarwal, A., Belgrave, D., Cho, K., and Oh, A. (eds.), *Advances in Neural Information Processing Systems*, volume 35, pp. 26565–26577. Curran Associates, Inc., 2022. URL [https://proceedings.neurips.cc/paper\\_files/paper/2022/file/a98846e9d9cc01cfb87eb694d946ce6b-Paper-Conference.pdf](https://proceedings.neurips.cc/paper_files/paper/2022/file/a98846e9d9cc01cfb87eb694d946ce6b-Paper-Conference.pdf).

Kidger, P. On neural differential equations, 2022. URL <https://arxiv.org/abs/2202.02435>.

Krizhevsky, A. and Hinton, G. Learning multiple layers of features from tiny images. Technical Report 0, University of Toronto, 2009.

Krizhevsky, A., Sutskever, I., and Hinton, G. E. Imagenet classification with deep convolutional neural networks. In Pereira, F., Burges, C., Bottou, L., and Weinberger, K. (eds.), *Advances in Neural Information Processing Systems*, volume 25. Curran Associates, Inc., 2012. URL [https://proceedings.neurips.cc/paper\\_files/paper/2012/file/c399862d3b9d6b76c8436e924a68c45b-Paper.pdf](https://proceedings.neurips.cc/paper_files/paper/2012/file/c399862d3b9d6b76c8436e924a68c45b-Paper.pdf).

Laine, S. and Aila, T. Temporal ensembling for semi-supervised learning. In *International Conference on Learning Representations*, 2017. URL <https://openreview.net/forum?id=BJ6oOfqge>.

Lee, J., Moradijamei, B., and Shakeri, H. Multi-marginal stochastic flow matching for high-dimensional snapshot data at irregular time points. In *Forty-second International Conference on Machine Learning*, 2025. URL <https://openreview.net/forum?id=ZLyb8DwXXE>.

Li, L., Hurault, S., and Solomon, J. Self-consistent velocity matching of probability flows. In *Thirty-seventh Conference on Neural Information Processing Systems*, 2023. URL <https://openreview.net/forum?id=C6fvJ2RfsL>.

Lin, Z., Khetan, A., Fanti, G., and Oh, S. Paegan: The power of two samples in generative adversarial networks. In Bengio, S., Wallach, H., Larochelle, H., Grauman, K., Cesa-Bianchi, N., and Garnett, S. (eds.), *Advances in Neural Information Processing Systems*, volume 33, pp. 12104–12114. Curran Associates, Inc., 2020. URL [https://proceedings.neurips.cc/paper\\_files/paper/2020/file/8d30aa96e72440759f74bd2306c1fa3d-Paper.pdf](https://proceedings.neurips.cc/paper_files/paper/2020/file/8d30aa96e72440759f74bd2306c1fa3d-Paper.pdf).

R. (eds.), *Advances in Neural Information Processing Systems*, volume 31. Curran Associates, Inc., 2018. URL [https://proceedings.neurips.cc/paper\\_files/paper/2018/file/288cc0ff022877bd3df94bc9360b9c5d-Paper.pdf](https://proceedings.neurips.cc/paper_files/paper/2018/file/288cc0ff022877bd3df94bc9360b9c5d-Paper.pdf).

Lipman, Y., Chen, R. T. Q., Ben-Hamu, H., Nickel, M., and Le, M. Flow matching for generative modeling. In *The Eleventh International Conference on Learning Representations*, 2023. URL <https://openreview.net/forum?id=PqvMRDCJT9t>.

Liu, X., Gong, C., and qiang liu. Flow straight and fast: Learning to generate and transfer data with rectified flow. In *The Eleventh International Conference on Learning Representations*, 2023. URL <https://openreview.net/forum?id=XVjTT1nw5z>.

Lu, C. and Song, Y. Simplifying, stabilizing and scaling continuous-time consistency models. In *The Thirteenth International Conference on Learning Representations*, 2025. URL <https://openreview.net/forum?id=LyJi5ugyJx>.

Lučić, M., Tschannen, M., Ritter, M., Zhai, X., Bachem, O., and Gelly, S. High-fidelity image generation with fewer labels. In Chaudhuri, K. and Salakhutdinov, R. (eds.), *Proceedings of the 36th International Conference on Machine Learning*, volume 97 of *Proceedings of Machine Learning Research*, pp. 4183–4192. PMLR, 09–15 Jun 2019. URL <https://proceedings.mlr.press/v97/lucic19a.html>.

Luhman, E. and Luhman, T. Knowledge distillation in iterative generative models for improved sampling speed, 2021. URL <https://arxiv.org/abs/2101.02388>.

Ma, C., Xiao, X., Wang, T., Wang, X., and Shen, Y. Learning straight flows: Variational flow matching for efficient generation, 2025. URL <https://arxiv.org/abs/2511.17583>.

Miyato, T., Kataoka, T., Koyama, M., and Yoshida, Y. Spectral normalization for generative adversarial networks. In *International Conference on Learning Representations*, 2018. URL <https://openreview.net/forum?id=B1QRgziT->.

Nichol, A. Q. and Dhariwal, P. Improved denoising diffusion probabilistic models, 2021. URL <https://openreview.net/forum?id=-NEXDKk8gZ>.

Ren, H., Zhao, S., and Ermon, S. Adaptive antithetic sampling for variance reduction. In Chaudhuri, K. and Salakhutdinov, R. (eds.), *Proceedings of the 36th International Conference on Machine Learning*, volume 97 of *Proceedings of Machine Learning Research*, pp. 5420–5428. PMLR, 09–15 Jun 2019. URL <https://proceedings.mlr.press/v97/ren19b.html>.

Reu, T., Dromigny, S., Bronstein, M. M., and Vargas, F. Gradient variance reveals failure modes in flow-based generative models. In *The Thirty-ninth Annual Conference on Neural Information Processing Systems*, 2025. URL <https://openreview.net/forum?id=pVaqdFlUAO>.

Rombach, R., Blattmann, A., Lorenz, D., Esser, P., and Ommer, B. High-resolution image synthesis with latent diffusion models. In *Proceedings of the IEEE/CVF Conference on Computer Vision and Pattern Recognition (CVPR)*, pp. 10684–10695, June 2022.

Sage, A., Timofte, R., Agustsson, E., and Gool, L. V. Logo synthesis and manipulation with clustered generative adversarial networks. In *2018 IEEE/CVF Conference on Computer Vision and Pattern Recognition*, pp. 5879–5888, 2018. doi: 10.1109/CVPR.2018.00616.

Salimans, T. and Ho, J. Progressive distillation for fast sampling of diffusion models. In *International Conference on Learning Representations*, 2022. URL <https://openreview.net/forum?id=TIdIXIpzhoI>.

Sauer, A., Schwarz, K., and Geiger, A. Stylegan-xl: Scaling stylegan to large diverse datasets. In *ACM SIGGRAPH 2022 Conference Proceedings*, SIGGRAPH '22, New York, NY, USA, 2022. Association for Computing Machinery. ISBN 9781450393379. doi: 10.1145/3528233.3530738. URL <https://doi.org/10.1145/3528233.3530738>.

Sohn, K., Berthelot, D., Carlini, N., Zhang, Z., Zhang, H., Raffel, C. A., Cubuk, E. D., Kurakin, A., and Li, C.-L. Fixmatch: Simplifying semi-supervised learning with consistency and confidence. In Larochelle, H., Ranzato, M., Hadsell, R., Balcan, M., and Lin, H. (eds.), *Advances in Neural Information Processing Systems*, volume 33, pp. 596–608. Curran Associates, Inc., 2020. URL [https://proceedings.neurips.cc/paper\\_files/paper/2020/file/06964dce9addb1c5cb5d6e3d9838f733-Paper.pdf](https://proceedings.neurips.cc/paper_files/paper/2020/file/06964dce9addb1c5cb5d6e3d9838f733-Paper.pdf).

Song, J., Meng, C., and Ermon, S. Denoising diffusion implicit models. In *International Conference on Learning Representations*, 2021a. URL <https://openreview.net/forum?id=St1giarCHLP>.

Song, Y. and Dhariwal, P. Improved techniques for training consistency models. In *The Twelfth International Conference on Learning Representations*, 2024. URL <https://openreview.net/forum?id=WNzy9bRDvG>.

Song, Y., Sohl-Dickstein, J., Kingma, D. P., Kumar, A., Ermon, S., and Poole, B. Score-based generative modeling through stochastic differential equations. In *International Conference on Learning Representations*, 2021b. URL <https://openreview.net/forum?id=PxTIG12RRHS>.

Song, Y., Dhariwal, P., Chen, M., and Sutskever, I. Consistency models. In *Proceedings of the 40th International Conference on Machine Learning*, ICML'23. JMLR.org, 2023.

Tong, A., FATRAS, K., Malkin, N., Huguet, G., Zhang, Y., Rector-Brooks, J., Wolf, G., and Bengio, Y. Improving and generalizing flow-based generative models with mini-batch optimal transport. *Transactions on Machine Learning Research*, 2024. ISSN 2835-8856. URL <https://openreview.net/forum?id=CD9Snc73AW>. Expert Certification.

Xiao, Z., Kreis, K., and Vahdat, A. Tackling the generative learning trilemma with denoising diffusion gans, 2022. URL <https://arxiv.org/abs/2112.07804>.

Yang, L., Zhang, Z., Song, Y., Hong, S., Xu, R., Zhao, Y., Zhang, W., Cui, B., and Yang, M.-H. Diffusion models: A comprehensive survey of methods and applications. *ACM Comput. Surv.*, 56(4), November 2023. ISSN 0360-0300. doi: 10.1145/3626235. URL <https://doi.org/10.1145/3626235>.

Yang, L., Zhang, Z., Zhang, Z., Liu, X., Liu, J., Xu, M., Meng, C., Ermon, S., Zhang, W., and CUI, B. Consistency flow matching: Defining straight flows with velocity consistency, 2025. URL <https://openreview.net/forum?id=bS76qaGbel>.

Zhai, S., ZHANG, R., Nakkiran, P., Berthelot, D., Gu, J., Zheng, H., Chen, T., Bautista, M. Á., Jaitly, N., and Susskind, J. M. Normalizing flows are capable generative models. In *Forty-second International Conference on Machine Learning*, 2025. URL <https://openreview.net/forum?id=2uheUFcFsM>.

Zhao, S., Liu, Z., Lin, J., Zhu, J.-Y., and Han, S. Differentiable augmentation for data-efficient gan training. In Larochelle, H., Ranzato, M., Hadsell, R., Balcan, M., and Lin, H. (eds.), *Advances in Neural Information Processing Systems*, volume 33, pp. 7559–7570. Curran Associates, Inc., 2020. URL [https://proceedings.neurips.cc/paper\\_files/paper/2020/file/55479c55ebd1efd3ff125f1337100388-Paper.pdf](https://proceedings.neurips.cc/paper_files/paper/2020/file/55479c55ebd1efd3ff125f1337100388-Paper.pdf).

Zheng, H., He, P., Chen, W., and Zhou, M. Truncated diffusion probabilistic models and diffusion-based adversarial auto-encoders. In *The Eleventh International Conference on Learning Representations*, 2023a. URL <https://openreview.net/forum?id=HDxgaKk9561>.

Zheng, K., Lu, C., Chen, J., and Zhu, J. Improved techniques for maximum likelihood estimation for diffusion odes. In *Proceedings of the 40th International Conference on Machine Learning*, ICML'23. JMLR.org, 2023b.

## A. Theoretical Analysis

### A.1. Preliminaries

Let  $p_0, p_1$  be distributions on  $\mathbb{R}^d$ . A probability path  $\{p_t\}_{t \in [0,1]}$  is *admissible* if there exists a measurable vector field  $u^* : \mathbb{R}^d \times [0, 1] \rightarrow \mathbb{R}^d$  such that  $(p_t, u_t^*)$  solves the continuity equation

$$\partial_t p_t(x) + \nabla \cdot (p_t(x) u_t^*(x)) = 0, \quad p_{t=0} = p_0, \quad p_{t=1} = p_1, \quad (3)$$

in the weak sense: for all  $\varphi \in C_c^\infty(\mathbb{R}^d)$ ,

$$\frac{d}{dt} \int \varphi(x) p_t(x) dx = \int \langle \nabla \varphi(x), u_t^*(x) \rangle p_t(x) dx.$$

Fix a path sampler  $\mathcal{P}$  inducing a joint law on  $(x_0, x_1, t)$  with  $t \sim \rho$  on  $[0, 1]$  and  $(x_0, x_1) \sim \pi$ , together with a measurable map  $\Phi : [0, 1] \times \mathbb{R}^d \times \mathbb{R}^d \rightarrow \mathbb{R}^d$  such that

$$x_t = \Phi_t(x_0, x_1), \quad (x_0, x_1, t) \sim \pi \otimes \rho.$$

Let  $u_t(x_0, x_1) \in \mathbb{R}^d$  denote a conditional target velocity (depending on the sampler). For a measurable predictor  $v : \mathbb{R}^d \times [0, 1] \rightarrow \mathbb{R}^d$  define the FM population risk

$$\mathcal{R}(v) := \mathbb{E} \|v(x_t, t) - u_t(x_0, x_1)\|_2^2. \quad (4)$$

**Lemma A.1** ( $L^2$  projection / regression form). *Let  $\mathcal{G}_t := \sigma(x_t, t)$  and assume  $\mathbb{E} \|u_t\|_2^2 < \infty$ . Then*

$$v^*(x, t) := \mathbb{E}[u_t(x_0, x_1) \mid x_t = x, t]$$

is the (a.s.) unique minimizer of  $\mathcal{R}(v)$  over all  $\mathcal{G}_t$ -measurable  $v$ , and

$$\mathcal{R}(v) - \mathcal{R}(v^*) = \mathbb{E} \|v(x_t, t) - v^*(x_t, t)\|_2^2. \quad (5)$$

*Proof.* Expand

$$\|v - u\|^2 = \|v - v^*\|^2 + \|v^* - u\|^2 + 2\langle v - v^*, v^* - u \rangle,$$

take conditional expectation given  $\mathcal{G}_t$  and use  $\mathbb{E}[u \mid \mathcal{G}_t] = v^*$  to kill the cross term; then average.  $\square$

Lemma A.1 shows that conditional flow matching is a *pointwise-in-time* regression problem: for each  $t$ , the predictor  $v(\cdot, t)$  is fit independently as an  $L^2$  projection. Crucially, the objective (4) imposes *no coupling across time*, so the learned vector field may exhibit arbitrary temporal oscillations even when achieving minimal population risk. The remainder of this appendix studies how introducing temporal coupling alters this geometry.

### A.2. TPC-FM as quadratic regularization in a trajectory-coupled Hilbert space

Rather than penalizing abstract smoothness in  $t$ , we regularize *discrepancies of predictions evaluated along the same sampled trajectory*. This enforces temporal coherence only on states that are jointly realizable under the path sampler, which is the relevant geometry for both optimization and sampling. Fix a pairing rule  $\psi : [0, 1] \rightarrow [0, 1]$  (possibly randomized; treat the randomness as absorbed into  $\rho$ ). Let  $t' = \psi(t)$  and define paired states  $(x_t, x_{t'}) = (\Phi_t(x_0, x_1), \Phi_{t'}(x_0, x_1))$ . Define the quadratic form

$$\|v\|_{\text{TPC}}^2 := \mathbb{E} \|v(x_t, t) - v(x_{t'}, t')\|_2^2. \quad (6)$$

Define the TPC-regularized population objective

$$\mathcal{R}_\lambda(v) := \mathcal{R}(v) + \lambda \|v\|_{\text{TPC}}^2, \quad \lambda > 0. \quad (7)$$

Let  $\mu$  denote the path marginal on  $(x, t)$ :  $d\mu(x, t) = p_t(x) \rho(t) dx dt$  and define the Hilbert space

$$\mathcal{H} := L^2(\mu; \mathbb{R}^d), \quad \langle f, g \rangle_{\mathcal{H}} = \int_0^1 \int \langle f(x, t), g(x, t) \rangle p_t(x) \rho(t) dx dt.$$

Define an operator  $\mathcal{A}_\psi$  on functions  $v$  by

$$(\mathcal{A}_\psi v)(x_0, x_1, t) := v(\Phi_t(x_0, x_1), t) - v(\Phi_{\psi(t)}(x_0, x_1), \psi(t)).$$

Then

$$\|v\|_{\text{TPC}}^2 = \mathbb{E} \|\mathcal{A}_\psi v\|_2^2, \quad (8)$$

i.e.,  $\|\cdot\|_{\text{TPC}}$  is the  $L^2(\pi \otimes \rho)$ -seminorm of  $\mathcal{A}_\psi v$ .

**Lemma A.2** (Tikhonov selection inequality). *Let  $v^* \in \arg \min \mathcal{R}(v)$  and  $v_\lambda \in \arg \min \mathcal{R}_\lambda(v)$ . Then*

$$\lambda \|v_\lambda\|_{\text{TPC}}^2 \leq \mathcal{R}(v^*) - \mathcal{R}(v_\lambda) \leq \mathcal{R}(v^*), \quad \Rightarrow \quad \|v_\lambda\|_{\text{TPC}}^2 \leq \frac{\mathcal{R}(v^*)}{\lambda}. \quad (9)$$

Moreover, if  $\mathcal{R}(v_\lambda) \leq \mathcal{R}(v^*) + \varepsilon$ , then

$$\|v_\lambda\|_{\text{TPC}}^2 \leq \inf_{v: \mathcal{R}(v) \leq \mathcal{R}(v^*) + \varepsilon} \|v\|_{\text{TPC}}^2 + \frac{\varepsilon}{\lambda}. \quad (10)$$

*Proof.* Optimality gives  $\mathcal{R}(v_\lambda) + \lambda \|v_\lambda\|_{\text{TPC}}^2 \leq \mathcal{R}(v^*) + \lambda \|v^*\|_{\text{TPC}}^2$ . Drop  $\lambda \|v^*\|_{\text{TPC}}^2 \geq 0$  to get (9). For (10), compare against any  $v$  with  $\mathcal{R}(v) \leq \mathcal{R}(v^*) + \varepsilon$ .  $\square$

Lemma A.2 formalizes TPC as a *selection principle*: among all predictors achieving near-minimal FM risk, the regularized objective prefers those with smaller temporal variation along coupled trajectories. This is the precise sense in which TPC reduces temporal oscillation at the population level.

### A.3. Anchor theorem: population regularization $\Rightarrow$ correlated gradients $\Rightarrow$ strict variance reduction

Let  $v_\theta$  be a parametric model. Define the per-sample FM loss and gradient

$$\ell(\theta; t, \xi) := \|v_\theta(x_t, t) - u_t(\xi)\|_2^2, \quad g(t, \xi) := \nabla_\theta \ell(\theta; t, \xi), \quad (11)$$

where  $\xi$  denotes the shared randomness producing  $(x_0, x_1)$  and any sampler noise, so that  $x_t = \Phi_t(\xi)$  and  $u_t = u_t(\xi)$ . Define the paired time  $t' = \psi(t)$  and  $h(t, \xi) := g(t', \xi)$ .

We now connect the regularized population view to stochastic optimization. Although TPC modifies the objective, its most immediate algorithmic effect is to *correlate gradient evaluations across time*, enabling classical variance-reduction mechanisms.

**Lemma A.3** (Optimal scalar control variate). *Let  $G, H$  be square-integrable random vectors in  $\mathbb{R}^m$  and consider  $\widehat{G}_\alpha := G - \alpha H$  with  $\alpha \in \mathbb{R}$ . Define scalar variance  $\text{Var}(Z) := \mathbb{E}\|Z - \mathbb{E}Z\|_2^2$  and covariance  $\text{Cov}(G, H) := \mathbb{E}\langle G - \mathbb{E}G, H - \mathbb{E}H \rangle$ . Then the minimizer is*

$$\alpha^* = \frac{\text{Cov}(G, H)}{\text{Var}(H)}, \quad (12)$$

and the minimum variance equals

$$\text{Var}(G - \alpha^* H) = \text{Var}(G) (1 - \rho^2), \quad \rho := \frac{\text{Cov}(G, H)}{\sqrt{\text{Var}(G)\text{Var}(H)}}. \quad (13)$$

*Proof.* Expand

$$\text{Var}(G - \alpha H) = \text{Var}(G) + \alpha^2 \text{Var}(H) - 2\alpha \text{Cov}(G, H),$$

optimize the quadratic in  $\alpha$  to get (12), then substitute and simplify to (13).  $\square$

We now derive a sufficient condition for  $\text{Cov}(g(t, \xi), g(t', \xi)) > 0$  from smoothness + path coupling.

Assume:

$$\exists L_\Phi < \infty : \mathbb{E}\|x_t - x_s\|_2^2 \leq L_\Phi^2 |t - s|^2, \quad \forall s, t \in [0, 1], \quad (14)$$

$$\exists L_g < \infty : \mathbb{E}\|g(t, \xi) - g(s, \xi)\|_2^2 \leq L_g^2 |t - s|^2, \quad \forall s, t \in [0, 1], \quad (15)$$

where (15) is implied by local Lipschitzness of  $v_\theta$  and bounded Jacobians on the path support.

**Lemma A.4** (Correlation lower bound from Lipschitz continuity). *Let  $G := g(t, \xi)$  and  $H := g(t', \xi)$  with  $t' = \psi(t)$ . Assume  $\mathbb{E}G = \mathbb{E}H$  (or work with centered versions) and  $\text{Var}(G) > 0$ . Then*

$$\text{Corr}(G, H) \geq 1 - \frac{\mathbb{E}\|G - H\|_2^2}{2\text{Var}(G)}. \quad (16)$$

Consequently, if  $\mathbb{E}\|G - H\|_2^2 \leq 2(1 - \rho_0)\text{Var}(G)$  for some  $\rho_0 \in (0, 1)$ , then  $\text{Corr}(G, H) \geq \rho_0$ .

*Proof.* For centered  $G, H$ ,

$$\mathbb{E}\|G - H\|_2^2 = \mathbb{E}\|G\|_2^2 + \mathbb{E}\|H\|_2^2 - 2\mathbb{E}\langle G, H \rangle = 2\text{Var}(G) - 2\text{Cov}(G, H),$$

hence  $\text{Cov}(G, H) = \text{Var}(G) - \frac{1}{2}\mathbb{E}\|G - H\|_2^2$  and dividing by  $\text{Var}(G)$  yields (16).  $\square$

The following result consolidates the preceding components into a single statement: population-level regularization, gradient correlation, and strict variance reduction are shown to be consequences of the same temporal coupling mechanism.

**Theorem A.5.** *Let  $v_\lambda \in \arg \min \mathcal{R}_\lambda(v)$ .*

*The key requirement for variance reduction is that gradients at paired times are positively correlated. We now show that this is not an ad-hoc assumption, but follows from smooth dependence on time together with path coupling induced by sharing the same endpoints  $(x_0, x_1)$ .*

Assume (14)–(15) and that the pairing  $\psi$  satisfies  $|t - \psi(t)| \leq \Delta$  a.s. for some  $\Delta \in (0, 1)$ . Then:

(i) **(Population contraction in the TPC metric)**

$$\|v_\lambda\|_{\text{TPC}}^2 \leq \frac{\mathcal{R}(v^*)}{\lambda}.$$

(ii) **(Quantitative correlation)** For  $G = g(t, \xi)$ ,  $H = g(\psi(t), \xi)$ ,

$$\mathbb{E}\|G - H\|_2^2 \leq L_g^2 \mathbb{E}|t - \psi(t)|^2 \leq L_g^2 \Delta^2,$$

hence by Lemma A.4,

$$\text{Corr}(G, H) \geq 1 - \frac{L_g^2 \Delta^2}{2\text{Var}(G)} =: \rho_0, \quad (17)$$

whenever the RHS is positive.

(iii) **(Strict variance reduction)** With  $\widehat{g}_\alpha := G - \alpha H$  and  $\alpha^*$  from Lemma A.3,

$$\text{Var}(\widehat{g}_{\alpha^*}) = \text{Var}(G)(1 - \rho^2) \leq \text{Var}(G)(1 - \rho_0^2) < \text{Var}(G),$$

for any  $\rho_0 \in (0, 1)$  satisfying (17).

*Proof.* (i) is Lemma A.2. (ii) uses (15) and  $|t - \psi(t)| \leq \Delta$ . (iii) is Lemma A.3 with the lower bound (17).  $\square$

The final step is to connect temporal regularity of the learned vector field to numerical behavior during probability-flow sampling. Since generation integrates the learned ODE only along states visited by the sampler, trajectory-wise temporal coherence is the relevant notion.

#### A.4. ODE link: TPC as control of temporal roughness and solver error

Let  $z_t$  solve the probability-flow ODE

$$\dot{z}_t = v_\theta(z_t, t), \quad z_0 \sim p_0, \quad (18)$$

and let  $\hat{z}_t$  be the explicit Euler discretization with step size  $h = 1/N$ :

$$\hat{z}_{k+1} = \hat{z}_k + h v_\theta(\hat{z}_k, t_k), \quad t_k = kh.$$

Assume  $v_\theta$  is Lipschitz in  $x$  with constant  $L_x$  and differentiable in  $t$  with  $\|\partial_t v_\theta(x, t)\|_2 \leq L_t$  on the region visited by  $(z_t, \hat{z}_t)$ .

**Lemma A.6** (Global error bound with explicit time-variation term). *There exists a constant  $C$  (depending on bounds on  $\|v_\theta\|$  and  $\|\nabla_x v_\theta\|$  on the trajectory tube) such that*

$$\|z_1 - \hat{z}_1\|_2 \leq e^{L_x} C h (1 + L_t). \quad (19)$$

*Proof sketch.* Write the local truncation error  $z_{t_{k+1}} - z_{t_k} - h v_\theta(z_{t_k}, t_k)$  and use Taylor expansion in time:

$$z_{t_{k+1}} = z_{t_k} + \int_{t_k}^{t_{k+1}} v_\theta(z_s, s) ds = z_{t_k} + h v_\theta(z_{t_k}, t_k) + \int_{t_k}^{t_{k+1}} [v_\theta(z_s, s) - v_\theta(z_{t_k}, t_k)] ds.$$

Bound the integrand by Lipschitz in  $x$  and  $t$ :

$$\|v_\theta(z_s, s) - v_\theta(z_{t_k}, t_k)\| \leq L_x \|z_s - z_{t_k}\| + L_t |s - t_k|,$$

and use Grönwall to accumulate.  $\square$

Lemma A.6 isolates temporal variation of the vector field as an explicit contributor to global discretization error. Thus, any mechanism that suppresses temporal roughness *along sampled trajectories* directly improves numerical stability at fixed step size.

For *local* pairings  $\psi(t) = t + \Delta$  with small  $\Delta$  (random or deterministic),

$$v(x_{t+\Delta}, t + \Delta) - v(x_t, t) = \Delta \partial_t v(x_t, t) + \Delta (\nabla_x v(x_t, t)) \dot{x}_t + O(\Delta^2),$$

hence (formally)

$$\frac{1}{\Delta^2} \mathbb{E} \|v(x_{t+\Delta}, t + \Delta) - v(x_t, t)\|_2^2 \approx \mathbb{E} \|\partial_t v(x_t, t) + (\nabla_x v(x_t, t)) \dot{x}_t\|_2^2. \quad (20)$$

Thus small  $\|v\|_{\text{TPC}}$  (for local  $\psi$ ) yields a small *trajectory-averaged* temporal derivative, which is exactly the quantity entering time-variation terms in discretization bounds such as (19). For global pairings (e.g. antithetic  $\psi(t) = 1 - t$ ),  $\|v\|_{\text{TPC}}$  still controls low-frequency temporal oscillations in a spectral sense (via the quadratic form induced by  $\mathcal{A}_\psi$ ), which again reduces effective temporal roughness on the sampler support.

#### A.5. Uniform convergence under TPC constraint

Let  $\mathcal{V}$  be a class of predictors bounded by  $\|v(x, t)\|_2 \leq B$  a.s. Define the constrained class  $\mathcal{V}_\tau := \{v \in \mathcal{V} : \|v\|_{\text{TPC}}^2 \leq \tau\}$ . For i.i.d. samples  $\{(x_0^i, x_1^i, t^i)\}_{i=1}^n$ , define the empirical risk

$$\hat{\mathcal{R}}(v) := \frac{1}{n} \sum_{i=1}^n \|v(x_{t^i}^i, t^i) - u_{t^i}(x_0^i, x_1^i)\|_2^2.$$

**Proposition A.7** (Rademacher bound for constrained class). *With probability  $\geq 1 - \delta$ ,*

$$\sup_{v \in \mathcal{V}_\tau} |\hat{\mathcal{R}}(v) - \mathcal{R}(v)| \leq c_1 \mathfrak{R}_n(\mathcal{V}_\tau) + c_2 B^2 \sqrt{\frac{\log(1/\delta)}{n}}, \quad (21)$$

for universal constants  $c_1, c_2 > 0$  and vector-valued Rademacher complexity  $\mathfrak{R}_n(\cdot)$ . In typical parameterizations,  $\mathfrak{R}_n(\mathcal{V}_\tau)$  is non-increasing in  $\tau$ .

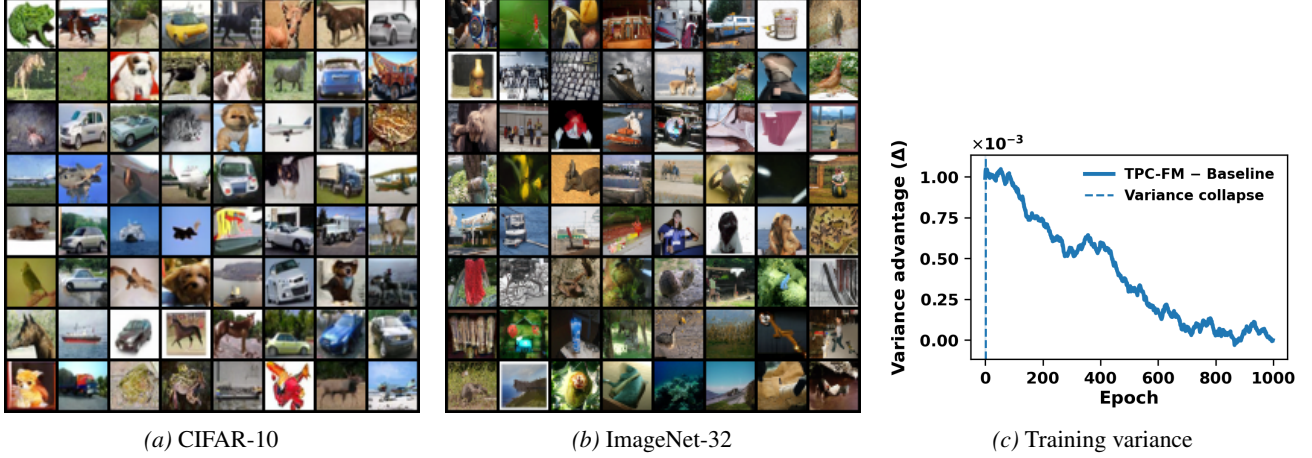


**Figure 3. Qualitative samples and training variance behavior.** CIFAR-10 and ImageNet-32 qualitative generations (left, middle), and training variance advantage of TPC-FM (right), where TPC-FM exhibits early variance collapse and sustained stability throughout training.

#### A.6. Limitations

No statement above directly implies monotone improvement in FID/IS:

$$\text{FID} = \text{FID}(\text{model bias, optimization error, solver error, estimation noise}),$$

and our results certify only the mechanism-level reductions:

$$\text{TPC} \Rightarrow \downarrow \|v\|_{\text{TPC}} \Rightarrow \begin{cases} \uparrow \text{Corr}(g(t, \xi), g(t', \xi)) \Rightarrow \downarrow \text{Var(SGD gradients)}, \\ \downarrow \text{temporal roughness on sampler support} \Rightarrow \downarrow \text{ODE discretization error}. \end{cases}$$

#### A.7. Takeaway

Under the stated assumptions,

$$v_\lambda \in \arg \min \mathcal{R}_\lambda \quad \Rightarrow \quad \|v_\lambda\|_{\text{TPC}}^2 \leq \frac{\mathcal{R}(v^*)}{\lambda},$$

and for paired-time gradients  $G = g(t, \xi), H = g(\psi(t), \xi)$ ,

$$\text{Var}(G - \alpha^* H) = \text{Var}(G)(1 - \rho^2) < \text{Var}(G) \quad \text{whenever } \rho > 0,$$

with  $\rho$  quantitatively lower bounded via Lemma A.4 under path-coupled Lipschitz regularity. Moreover, for sampling  $\dot{z}_t = v_\theta(z_t, t)$ , Euler-type global error contains explicit dependence on temporal variation (Lemma A.6), which is controlled in a trajectory-averaged sense by local TPC penalties through (20).

## B. Generated Samples

Table 8. Comparison of GAN, ODE, and SDE generative models on CIFAR-10 under one-step and full-simulation settings.

Method	NFE (↓)	IS (↑)	FID (↓)	Recall (↑)
<b>GAN</b>				
SNGAN (Miyato et al., 2018)	1	8.22	21.7	0.44
StyleGAN2 (Karras et al., 2020)	1	9.18	8.32	0.41
StyleGAN-XL (Sauer et al., 2022)	1	-	1.85	0.47
StyleGAN2 + ADA (Karras et al., 2020)	1	9.40	2.92	0.49
StyleGAN2 + DiffAug (Zhao et al., 2020)	1	9.40	5.79	0.42
TransGAN + DiffAug (Jiang et al., 2021)	1	9.02	9.26	0.41
<b>GAN with U-Net</b>				
TDPM (T=1) (Zheng et al., 2023a)	1	8.65	8.91	0.46
Denoise. Diff. GAN (T=1) (Xiao et al., 2022)	1	8.93	14.6	0.19
<b>ODE</b> <i>One-Step Generation (Euler solver; N=1)</i>				
DDIM Distillation (Luhman & Luhman, 2021)	1	8.36	9.36	0.51
NCSN++ (VE ODE; Distill) (Song et al., 2021b)	1	2.57	2.54	0.0
Progressive (Salimans & Ho, 2022)	1	-	9.12	-
DDIM (Song et al., 2021a)	1	-	> 20	-
<b>ODE</b> <i>Full Simulation (Runge–Kutta RK45), Adaptive N</i>				
NCSN++ (VE ODE) (Song et al., 2021b)	176	9.35	5.38	0.56
<b>SDE</b> <i>Full Simulation (Euler solver)</i>				
DDPM (Ho et al., 2020)	1000	9.46	3.21	0.57
NCSN++ (VE SDE) (Song et al., 2021b)	2000	9.83	2.38	0.59
<b>ODE</b> <i>Full Simulation (Euler solver)</i>				
DDIM (Song et al., 2021a)	10	-	13.36	-
DDIM (Song et al., 2021a)	100	-	4.16	-